高温水中で生成したステンレス鋼の表面皮膜の3次元アトムプローブトモグラフィー

3-D atom-probe tomography of surface oxides in stainless steels formed under high-Temperature water

Sergio Lozano-Perez *1, David Saxey *1,
Takuyo Yamada *2 and Takumi Terachi *2

要約　加圧水型一次冷却材環境下のステンレス鋼の酸化は，高温高圧水中で生じる複雑な現象として知られる．本報告では，アトムプローブ　トモグラフィーが，原子スケールで酸化物の化学的性質を理解するために必要な高空間分解能で且つ高い分析感度を併せ持つことを実証する．表面酸化に及ぼす冷間加工の影響についても調べ，また議論する．

キーワード　加圧水型原子力発電所，表面酸化，ステンレス鋼，3次元アトムプローブ　トモグラフィー，冷間加工

Abstract　The oxidation of stainless steels under Pressurized Water Reactor（PWR）primary water conditions is a complex phenomenon since it occurs at high pressure, high temperature and in the presence of a complex water chemistry. In this paper we demonstrate that atom-probe tomography combines the high spatial resolution and chemical sensitivity required to understand the chemistry of oxidation at the atomic scale. Effects of cold work in surface oxidation have also been characterized and will be discussed.

Keywords　pressurized water reactor, surface oxidation, stainless steels, 3-D atom-probe tomography, cold-work

1. Introduction

Low potential stress corrosion cracking（LPSCC）of stainless steels is a very important degradation phenomenon in pressurized water reactors（PWRs）. Autoclave testing under controlled environments confirmed that highly cold-worked stainless steels are susceptible to SCC even in PWR primary water conditions [1] and, recently, it was reported in operating PWR plants [2]. In order to clarify the corrosion mechanisms and the role of cold work, it is important to characterize the surface oxides formed, as well as the oxide-matrix interface, with the highest level of detail.

Chemical characterization of oxide layers has been traditionally performed with X-ray Photoemission Spectroscopy（XPS）[3]～[5], Auger Electron Spectroscopy（AES）[6]～[8], Secondary Ion Mass Spectroscopy（SIMS）[9]～[13], direct current glow discharge mass spectrometry [14], Raman spectroscopy [15] or Transmission Electron Microscopy（TEM）[16]～[19]. When lateral resolution is the critical parameter, TEM or Scanning TEM（STEM）can extract information from areas smaller than 1 nm, however, the microanalytical techniques available, Energy Dispersive Spectroscopy（EDS）or Electron Energy Loss Spectroscopy（EELS）, have limited sensitivities and struggle to detect minor impurities in the ppm concentration. Other techniques, such as SIMS, can perform better in terms of detectability limits, but they lack lateral

＊1　Department of Materials, University of Oxford, Parks Road, Oxford, OX1 3PH, UK
＊2　INSS, 64 Sata, Mihama-cho, Mikata-gun, Fukui 919-1205, Japan

resolution. Three-dimensional(3-D)information can be obtained from some techniques such as XPS, AES and SIMS in the form of depth-profiling combined with mapping, or STEM using electron tomography. In the case of electron tomography, the best 3-D spatial resolution can be achieved with voxels as little as $1nm^3$[20][21]. The only reference to the use of atom-probe tomography to understand surface oxidation in stainless steels in the literature is based on high-temperature oxidation in air of polished needles[22].

The characterization of surface oxidation in cold-worked samples requires high lateral and depth resolution, in order to reveal how the defects created by the CW interact with the oxidation process, as well as high chemical sensitivity, in order to investigate the role of minor impurities. Modern atom-probe instruments can detect concentrations of 10ppm, with equal sensitivity across all species, including light elements such as oxygen and lithium. Under suitable conditions this chemical sensitivity is combined with sub-nanometre spatial resolution, making it the ideal technique for providing this type of information.

It is well known that the oxide films formed in steels under PWR primary water conditions consist of a double-layer structure, with an inner Cr-rich spinel and an outer Fe-rich spinel layer[23]. Recent studies by Terachi and co-workers have characterized the influence of cold-work and Cr-content amongst other parameters[1][6][19][24]~[26].

2. Materials

In this research, the oxidation behaviour of 20% CW 316 SS was characterized. Coupon specimens were cold-worked before autoclave testing. Specimens were miller-polished and degreased with acetone and then immersed in the autoclave under simulated PWR primary water(500ppm B + 2ppm Li + 30cc-STP/kg H_2O)for 1500h at 340℃ . After the test, the specimen developed a Cr-rich spinel inner oxide of ~200nm in thickness. The composition of the 316 alloy was, in weight % , 0.051 C, 0.51 Si, 1.48 Mn, 0.028 P, 0.001 S, 13.2 Ni, 2.34 Mo, 16.47 Cr and balance of Fe.

3. Methodology

In order to extract needle-shaped specimens containing the oxide-metal interface, the coupon specimens were cross-sectioned. The cross-sectional surface was subsequently mirror polished mechanically, down to colloidal silica. A FEI 200 single-beam FIB equipped with an in-situ micromanipulator was used for the sample extraction and a Zeiss NVision 40 FIB/SEM was used for the tip sharpening. When the bulk sample was first put in the FIB, a layer of Pt was deposited over the surface oxide where the sample is going to be extracted from, using a current of 100pA Ga+. Next, the cross-sectional surface next to the deposited Pt is further polished with the Ga+beam (down to 100pA Ga+). This helped to reveal the microstructure and confirm that the oxide layer was present under the deposited Pt, as can be observed in Figure 1. Finally, a 25μm long specimen was extracted from the bulk sample as shown in Figure 2. The outer end of the specimen contained the oxide-metal interface. A detailed description of this procedure can be found in[27]~[29]. The specimen is then welded to a dedicated Cu post made by Fischione(See Figure 3).

At this point, the sample is moved to the Zeiss FIB for the final polishing. A series of annular masks with decreasing current and inner radii is placed around the top of the sample, gradually milling the tip to a needle-shape with a final diameter smaller than 200nm. In Figure 4, an image taken near the end of the polishing procedure reveals the level of detail that can be observed with the electron gun and the in-lens detector in the NVision FIB/SEM.

The surface-oxide specimens were analysed in a LEAP® 3000X HR atom probe using~10ps laser pulses to stimulate field evaporation. The laser spot

Figures

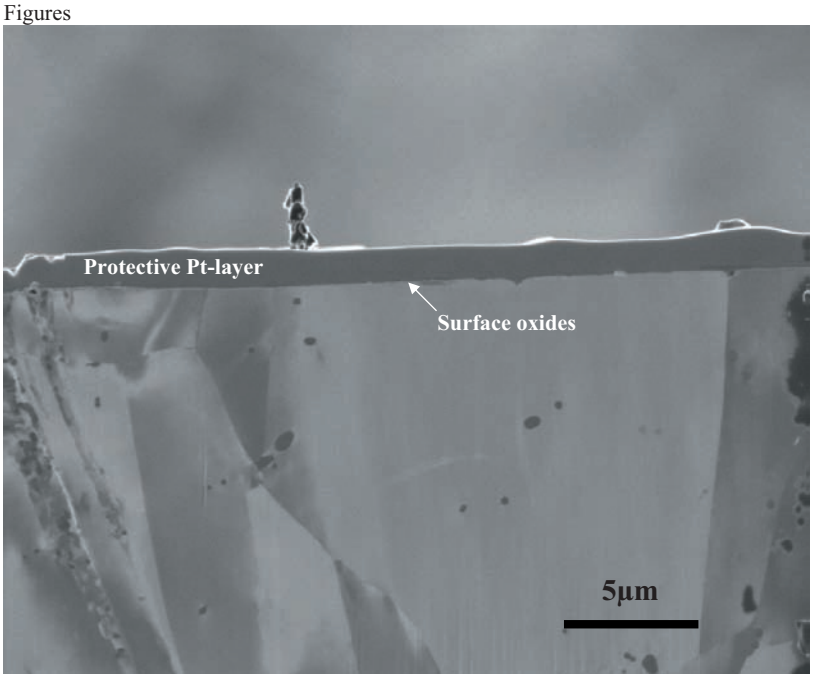

Figure 1. FIB SE image showing the cross-sectional area of the sample with a Pt layer deposited on top to preserve the surface oxides during sample preparation.

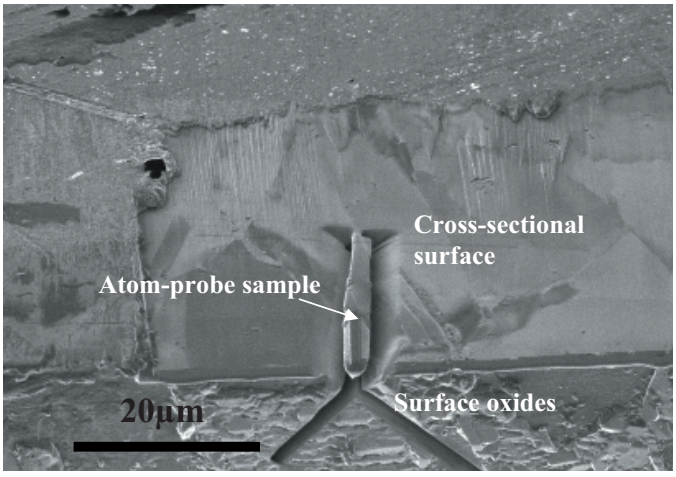

Figure 2. FIB SE image showing how the post containing the surface oxides is milled from the sample

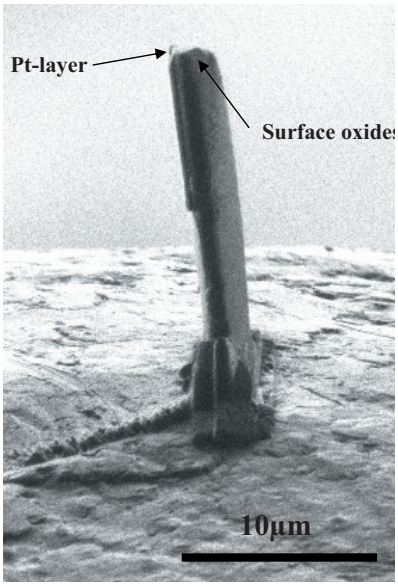

Figure 3. FIB SE image showing the specimen post welded on a Fischione post ready for the final sharpening

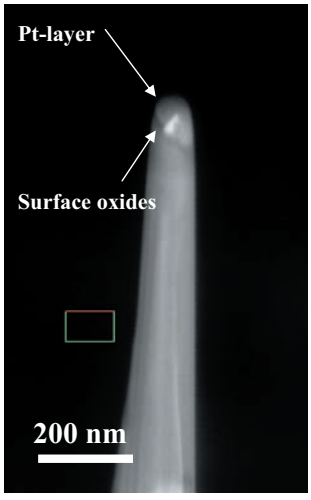

Figure 4. SEM in-lens image showing the atom-probe sample at the latest stages of polishing. The Cr-rich oxide appears as a darker band below the remaining Pt-layer at the top.

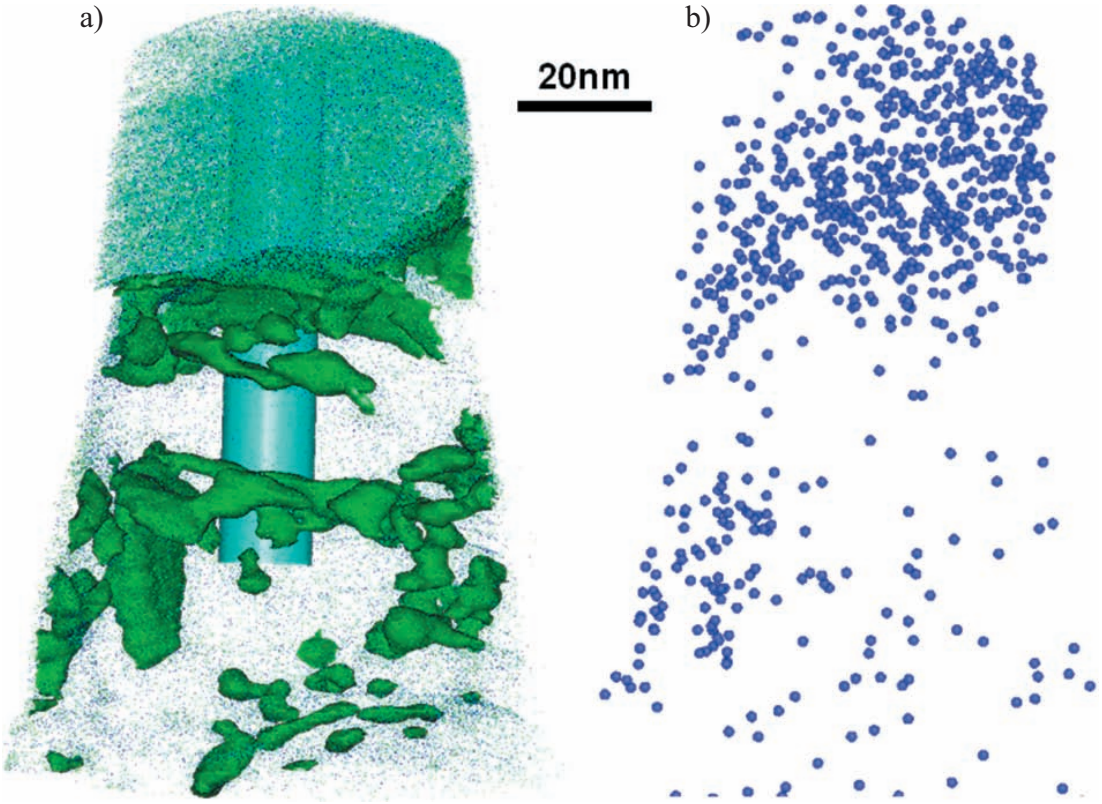

Figure 5. Atom maps showing the distribution of (a) Cr and Fe atoms within oxides (green-blue dots) and (b) lithium atoms (blue spheres). The isoconcentration surface in (a) corresponds to a concentration of approximately 10% oxide species. The cylinder in (a) shows the region from which the 1-D concentration profile (below) was generated.

was approximately 5-10μm in diameter, with a wavelength of 532nm, a pulse rate of 160kHz, and 0.6-0.7nJ per pulse. Ions were field-evaporated from the specimens to give an average detection rate of 0.01 ions per pulse. The specimen base-temperature was 65K during the analyses.

TEM samples containing the surface oxides were prepared in the FEI 200 FIB from the same bulk materials following the procedure described in [30]~[32]. EELS characterization was performed in a JEOL 3000F equipped with a Gatan GIF and operated at 297kV. The microscope was operated in STEM mode using a 150 pA probe with a 12mrad half-convergence angle and 9mrad half-collection angle. EELS quantification was performed using the inelastic cross-section values (with the Hartree-Slater approximation) provided by the EELS quantification routine in Gatan's Digital Micrograph.

4. Results

316SS oxidized under simulated PWR primary water conditions developed a dual oxide layer with an inner layer of Cr-rich spinel and an outer layer of Fe-rich spinel [33] [34]. With the addition of the microstructure caused by the cold-work, the oxidation process is more complex and enhanced oxidation of twin deformation bands has been observed [13] [26]. Since the total width of the oxide layers (Fe-rich plus Cr-rich) exceeds the depth of analysis that can be realistically achieved with the atom-probe, only the Cr-rich oxide layer was analyzed. For this reason, the oxide-metal interface was intentionally left close to the apex of the tip so it can also be analyzed.

The reconstructed dataset after atom-probe evaporation can be seen in Figure 5. In order to simplify the representation, since more than 10 million atoms were collected, only the oxide has been represented in Figure 5a. The inner Cr-rich surface oxide is clearly visible at the top of the sample, while the Cr-rich oxide intrusions, following microstructural features created by the cold work, have been rendered as isosurfaces for ease of view. In Figure 5b, a 3-D reconstruction revealing the location of the Li atoms can be seen. A 1-D line profile has been extracted from the dataset at the location marked by the cylinder in Figure 5a.

5. Discussion

In recent years, the introduction of commercial systems capable of operating in laser-pulsed evaporation mode [35] ~ [37], has enabled routine characterization of non-conductive samples in the atom-probe. Also, recent advances in the instrumentation [38] [39] have greatly increased both the lateral field-of-view and the speed at which data can be collected, leading to a greater than 100-fold increase in the volume of material that can be analysed within a day. At the same time, modern dual-beam FIBs have provided the required precision in the sample preparation to design the type of specimen described in this paper. For the first time, cold-worked samples containing real surface oxides have been successfully prepared and characterized in the atom-probe. The evaporation of samples containing oxides or interfaces, however, is not a simple phenomenon and its analysis must be approached with great care. For example, the different evaporation fields for the oxide and matrix can lead to distortions in the reconstructed interface area. The interpretation of the transition region in profiles such as in Figure 6 is not straightforward. Also, when oxidized species are evaporated, they can reach the detector as a single atom (e.g. metal or oxygen) or as a molecular combination of metal and oxygen atoms. It is therefore challenging to ensure that all elements have been fully accounted for in the final quantification.

In order to ensure that quantitative data was consistent, a cross-sectional TEM sample containing the surface oxides and the metal-oxide interface was prepared from the same specimens and characterized using EELS. The region chosen for the 316SS sample is shown in Fig 7, together with the line profile across the oxide-metal interface. Quantitative results obtained after processing the EELS data are shown in Figure 8. As can be seen, the atom-probe concentrations shown in the line profile in Figure 6 match very well those obtained by electron energy loss spectroscopy. The only inconsistency occurs when following the Mn concentration across the oxide-metal interface. In the EELS line-profile, the Mn signal falls to almost zero in the metal. This behaviour has been identified as an artefact due to the increase in sample thickness after the interface. The extra thickness allows for some multiple scattering to occur which has a dual detrimental effect. First, it changes the shape of the Mn L23 pre-edge, preventing a satisfactory fitting with an inverse power-law curve. Second, it spreads out the already weak Mn signal.

The data also reveals for the first time, the location of lithium atoms coming from the primary water, which are incorporated into the Cr-rich spinel. Boron was not observed in this region. However the local detection limit for boron was approximately 15ppm, which was higher than in the metal due to excess noise during evaporation of the oxide. It should be noted that prior NanoSIMS characterization of the same oxide layer [13] suggested that Boron might be present only at the outer part of the Cr-rich spinel layer, which was intentionally milled away during FIB sample preparation of the atom-probe needle.

As can be seen in Figure 5a, the oxidation did not stop at the oxide-metal interface and progressed beyond this point, benefiting from the highly deformed microstructure caused by the cold work. When the sample was characterized using STEM HAADF, similar pockets of oxidation below the

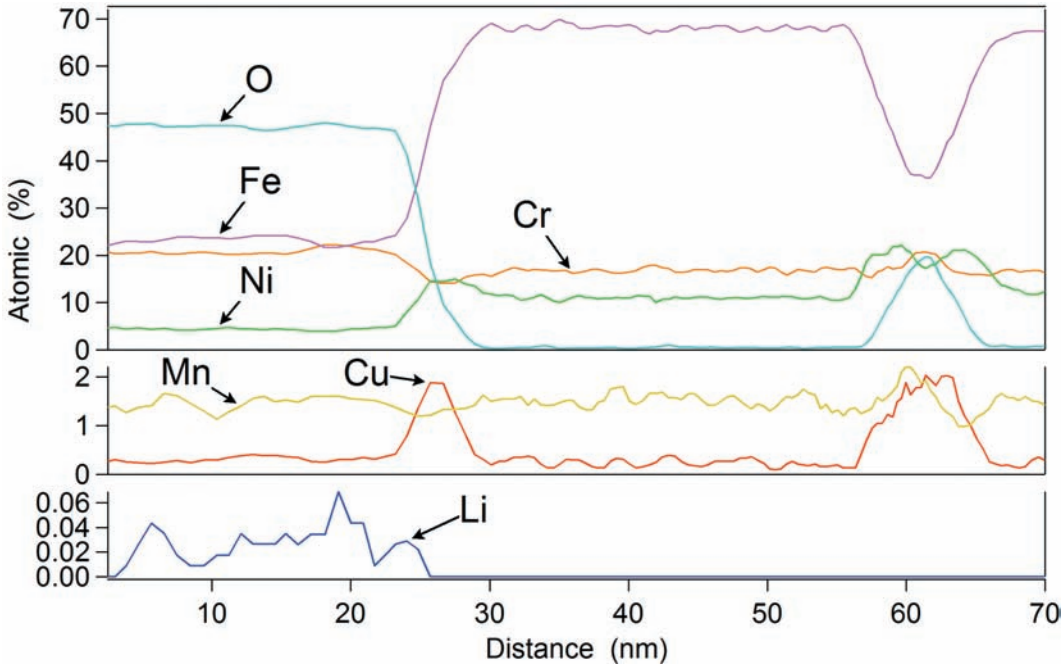

Figure 6. 1-D concentration profile across oxide-metal interface. Region of analysis shown in previous figure. All molecular ions are decomposed into their constituent atomic species. Si, Mo and C are not shown. The left side of the profile corresponds to the surface oxide. The O-rich region on the right side is a sub-surface feature.

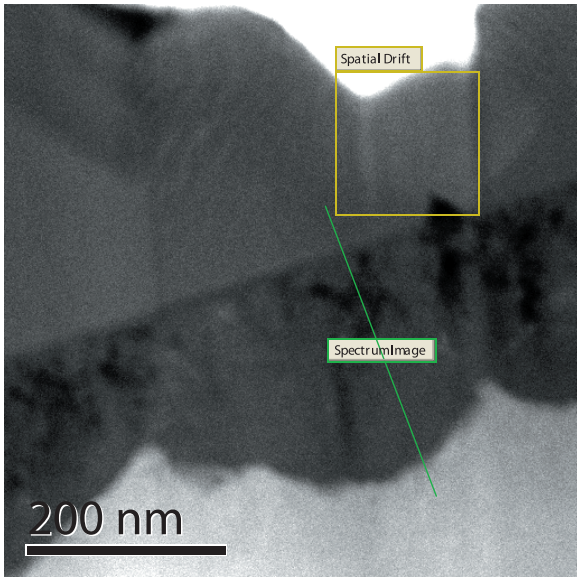

Figure 7. HAADF image showing a cross-sectional TEM sample from the 316SS specimen and the location of the EELS line profile

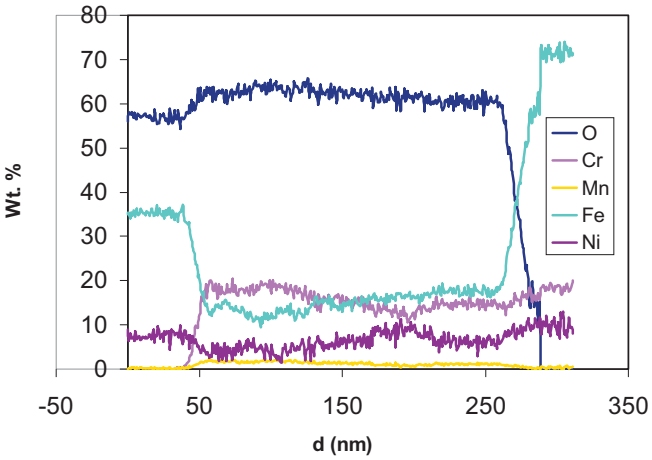

Figure 8. Quantitative EELS line profile across the oxide layers and the oxide-metal interface in the 316 sample. Location of line profile is shown in Figure 7.

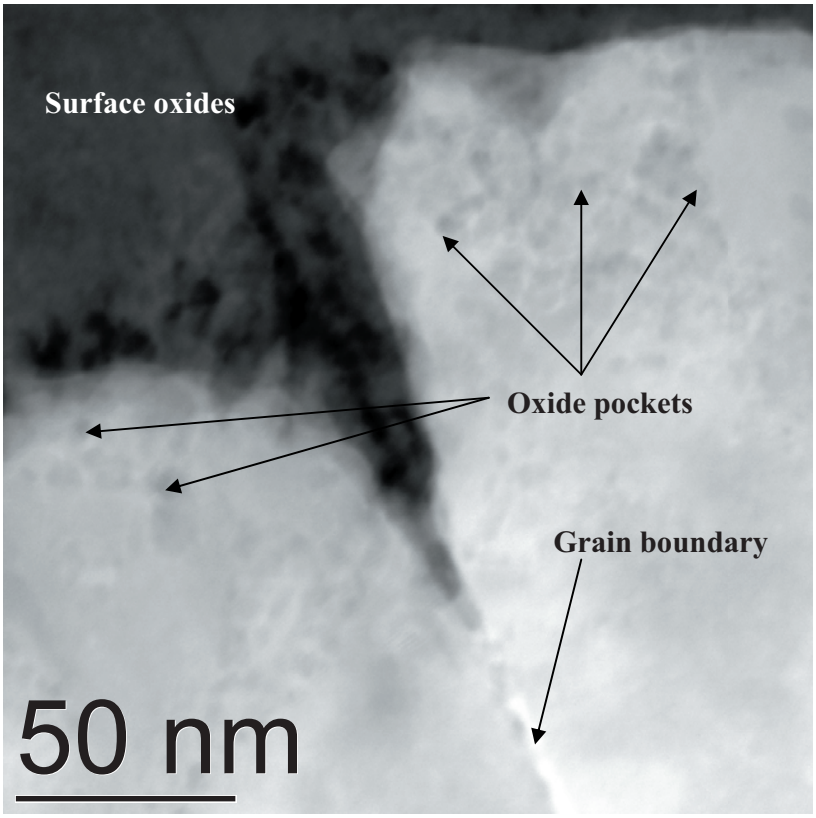

Figure 9. STEM HAADF image showing localized oxidation at a grain boundary intersecting the surface exposed to the environment. Cr-rich spinel (darker) is at the top and metallic matrix (brighter) is at the bottom. The darker localized areas below the interface were identified as pockets of oxide (only a few of them have been arrowed).

oxide-metal interface were observed (see Fig. 9). Understanding the oxidation mechanisms of cold-work austenitic stainless steels will be very valuable in order to understand SCC mechanisms, since it illustrates how the cold work locally modifies the original corrosion behaviour of the alloy.

6. Conclusions

This work has demonstrated that atom-probe tomography can be efficiently used to characterize surface oxides in stainless steels produced under simulated PWR primary water conditions. The high chemical sensitivity of the atom-probe allows the detection and quantification of Li incorporated into the inner Cr-rich oxide layer. The high spatial resolution in three dimensions has also allowed the visualization of the complex oxidation processes that occur near the oxide-metal interface in cold-worked samples. It is expected that this technique will play an important role in the future clarification of the oxidation mechanisms of these alloys.

7. Acknowledgements

Sergio Lozano-Perez is grateful to INSS and the Department of Materials (University of Oxford) for sponsoring this research. The atom probe analysis was conducted within the Opal UK Atom Probe Facility at the University of Oxford — funded by the UK Engineering and Physical Sciences Research Council (EPSRC) under grant no. EP/077664/1.

8. References

(1) K. Arioka, T. Yamada, T. Terachi *et al.*, "Intergranular stress corrosion cracking behavior of austenitic stainless steels in hydrogenated high-temperature water," Corrosion **62**, pp.74-83, (2006).

（2）T. Couvant, L. Legras, C. Pokor, *et al*. "Investigations on the mechanisms of PWSCC of strain hardened austenitic stainless steels," 499-514.

（3）Z. Homonnay, E. Kuzmann, K. Varga *et al.*, "Comprehensive investigation of the corrosion state of the heat exchanger tubes of steam generators. Part II. Chemical composition and structure of tube surfaces" J. Nucl. Mater. **348**, pp. 191-204, (2006).

（4）J. C. Langevoort, I. Sutherland, L. J. Hanekamp *et al.*, "On the oxide formation on stainless steels AISI 304and Incoloy 800H investigated with XPS," Appl. Surf. Sci. **28** pp. 167-179, (1987).

（5）S. B. Couling, L. S. Welch, "Characterization by XPS and AES of oxide films formed on stainless steel 304 under various PWR conditions," Surf Interface Anal **12**, pp. 412-418, (1988).

（6）T. Terachi, T. Yamada, T. Miyamoto *et al.*, "Corrosion behavior of stainless steels in simulated PWR primary water -effect of chromium content in alloys and dissolved hydrogen-," J Nucl Sci Technol **45**, pp. 975-984, (2008).

（7）M. F. Montemor, M. G. S. Ferreira, M. Walls*et al.*, "Influence of pH on properties of oxide films formed on type 316L stainless steel, alloy 600, and alloy 690 in high-temperature aqueous environments," Corrosion **59**, pp. 11-21, (2003).

（8）G. C. Allen, R. K. Wild,M. Weiss, "CHARACTERIZATION OF THE OXIDE-METAL INTERFACE AT THE SURFACE OF A STAINLESS STEEL," Philosophical Magazine A: Physics of Condensed Matter, Structure, Defects and Mechanical Properties **48**, pp. 373-386, (1983).

（9）P. Marriott, S. B. Couling,P. R. Chalker, "High spatial resolution SIMS investigation of oxides formed on stainless steel under PWR conditions," Appl. Surf. Sci. **37**, pp. 217-232, (1989).

(10) T. Honda, A. Minato, K. Ohsumi *et al.*, "DEPOSITION OF RADIOACTIVE IONS ON BOILING WATER REACTOR COMPONENT MATERIALS," Corrosion **43**, pp. 179-185, (1987).

(11) J. C. Vickerman, "Static sims - A technique for surface chemical characterisation in basic and applied surface science," Surf. Sci. **189-190**, pp. 7-14, (1987).

(12) S. Lozano-Perez, M. R. Kilburn, T. Yamada *et al.*, "High-resolution imaging of complex crack chemistry in reactor steels by Nano-SIMS" J Nuc Mat **374**, pp. 61-68, (2008).

(13) S. Lozano-Perez, M. Schröder, T. Yamada *et al.*, "Using NanoSIMS to map trace elements in stainless steels from nuclear reactors" App Surf Sci **255**, pp. 1541, (2008).

(14) L. O. Actis-Dato, L. A. De Las Heras, M. Betti *et al.*, "Investigation of mechanisms of corrosion due to diffusion of impurities by direct current glow discharge mass spectrometry depth profiling," J. Anal. at. Spectrom. **15**, pp. 1479-1484, (2000).

(15) J. H. Kim, I. S. Hwang, "Development of an in situ Raman spectroscopic system for surface oxide films on metals and alloys in high temperature water," Nucl. Eng.Des. **235**, pp. 1029-1040, (2005).

(16) J. Bentley, S. R. Gilliss, C. B. Carter *et al.*, "Nanoscale EELS analysis of oxides: composition mapping, valence determination and beam damage," Journal of Physics: Conference Series **26**, pp. 69-72, (2006).

(17) K. Fujii, K. Fukuya, N. Nakajima, "Characterization of SCC crack tip in alloy 600 in simulated primary water of PWR," Proceedings of the 3rd International Symposium on Materials Chemistry in Nuclear Environment (Material Chemistry MC'02). (13-15 March 2002) Tsukuba, Japan. (2002).

(18) S. M. Bruemmer, L. E. Thomas, "High-resolution analytical electron microscopy characterization of corrosion and cracking at buried interfaces," Surface and Interface Analysis **31**, pp. 571-581, (2001).

(19) T. Terachi K. Arioka. in: "Characterization

of Oxide Film Behaviors on 316Stainless Steels in High-Temperature Water - Influence of Hydrogen and Oxygen Considerations for Initiation of SCC -" Proceedings of the Corrosion 2006 61st Annual Conference and Exposition, 12-16 March, (2006).

(20) M. Weyland, P. A. Midgley, "Extending Energy-Filtered Transmission Electron Microscopy (EFTEM) into Three Dimensions Using Electron Tomography," Microscopy and Microanalysis **9**, pp. 542-555, (2003).

(21) M. Weyland, P. A. Midgley, "Electron tomography," Materials Today **7**, pp. 32-40, (2004).

(22) S. Ohkido, Y. Ishikawa, T. Yoshimura, "POSAP analysis of the oxide-alloy interface in stainless steel," Appl. Surf. Sci. **76-77**, pp. 261-265, (1994).

(23) J. Robertson, "The mechanism of high temperature aqueous corrosion of steel," Corros. Sci. **29**, pp. 1275-1291, (1989).

(24) T. Terachi K. Arioka.: "Influence of dissolved hydrogen, boric acid and Cr concentration on oxide film of SUS316 under high-temperature water," Proceedings of conference on water chemistry of nuclear reactor systems, October, San Francisco, P. 128, (2004).

(25) T. Terachi, K. Fujii,K. Arioka, "Microstructural characterization of SCC crack tip and oxide film for SUS 316 stainless steel in simulated PWR primary water at 320 degrees C," J Nucl Sci Technol **42**, pp. 225-232, (2005).

(26) T. Terachi, T. Yamada, G. Chiba, *et al*. "Influence of cold work on IGSCC of 316 stainless steel in hydrogenated high-temperature water" CORROSION/2007. Paper 7605. (2007).

(27) K. Thompson, D. Lawrence, D. J. Larson *et al.*, "In situ site-specific specimen preparation for atom probe tomography" Ultramicroscopy **107**, pp. 131-139, (2007).

(28) S. Lozano-Perez, "A guide on FIB preparation of samples containing stress corrosion crack tips for TEM and atom-probe analysis," Micron **39**, pp. 320-328, (2008).

(29) D. W. Saxey, J. M. Cairney, D. McGrouther*et al.*, "Atom probe specimen fabrication methods using a dual FIB/SEM" Ultramicroscopy **107**, pp. 756-760, (2007).

(30) L. A. Giannuzzi, J. L. Drown, S. R. Brown *et al.*, "Applications of the FIB lift-out technique for TEM specimen preparation," Microsc. Res. Tech. **41**, pp. 285-290, (1998).

(31) S. Lozano-Perez, Y. Huang, R. Langford *et al.*, "Preparation of TEM specimens containing stress corrosion cracks in austenitic alloys using FIB" IoP Conf Ser **168**, p. 191(2001).

(32) R.M. Langford, D. Ozkaya, C. Kaufman, et al., "Assessment of different focused ion beam milling conditions for the preparation of TEM cross-sections for high-resolution electron microscopy," Electron Microscopy and Analysis 2001. Proceedings. Dundee, (5-7 Sept. 2001.) UK. (2001).

(33) J. Robertson, "Modelling of corrosion and corrosion release in PWR primary circuits," *Water Chemistry of Nuclear Reactor Systems 5. Proceedings of the International Conference. Bournemouth, UK. Royal Soc. Chem. Eur. Nucl. Soc. Instn. Chem. Eng.23-27 Oct. 1989.* p. 254.

(34) T. Terachi, T. Yamada, K. Arioka, *et al*. "Role of corrosion in LPSCC of Fe-and Ni-based alloys," Proceedings of the International Symposium on Research for Ageing Management of Light Water Reactors, Oct. pp. 22-23, (2007).

(35) B. Gault, F. Vurpillot, A. Vella *et al.*, "Design of a femtosecond laser assisted tomographic atom probe," Rev. Sci. Instrum. **77** (2006).

(36) F. Vurpillot, B. Gault, A. Vella *et al.*, "Estimation of the cooling times for a metallic tip under laser illumination," Appl. Phys. Lett. **88**(2006).

(37) A. Cerezo, G. D. W. Smith,P. H. Clifton, "Measurement of temperature rises in the femtosecond laser pulsed three-dimensional

atom probe," Appl. Phys. Lett. **88**(2006).
(38) T. F. Kelly, T. T. Gribb, J. D. Olson *et al.*, "First data from a commercial local electrode atom probe (LEAP)," Microscopy and Microanalysis **10**, pp. 373-383, (2004).
(39) T. F. Kelly, M. K. Miller, "Invited review article: Atom probe tomography" Rev. Sci. Instrum.; Rev. Sci. Instrum. **78**(2007).